Earth and Planetary Science Letters 533 (2020) 115976

Contents lists available at ScienceDirect

Earth and Planetary Science Letters

www.elsevier.com/locate/epsl

Extensive marine anoxia associated with the Late Devonian Hangenberg Crisis

Feifei Zhang [a,b,c,*], Tais W. Dahl [b], Timothy M. Lenton [d], Genming Luo [e], Shu-zhong Shen [a], Thomas J. Algeo [e,f,g], Noah Planavsky [c], Jiangsi Liu [e], Ying Cui [h], Wenkun Qie [i], Stephen J. Romaniello [j], Ariel D. Anbar [j,k]

[a] School of Earth Sciences and Engineering, Nanjing University, 163 Xianlin Avenue, Nanjing 210023, China
[b] Globe Institute, University of Copenhagen, København K, Denmark
[c] Department of Geology and Geophysics, Yale University, New Haven, CT 06511, USA
[d] Global Systems Institute, University of Exeter, Exeter EX4 4QE, UK
[e] State Key Laboratory of Biogeology and Environmental Geology, China University of Geosciences, Wuhan, Hubei 430074, China
[f] State Key Laboratory of Geological Processes and Mineral Resources, China University of Geosciences, Wuhan, Hubei 430074, China
[g] Department of Geology, University of Cincinnati, Cincinnati, OH 45221-0013, USA
[h] Department of Earth and Environmental Studies, Montclair State University, Montclair, NJ 07043, USA
[i] State Key Laboratory of Palaeobiology and Stratigraphy, Nanjing Institute of Geology and Palaeontology and Center for Excellence in Life and Palaeoenvironment, Chinese Academy of Sciences, Nanjing 210008, China
[j] School of Earth and Space Exploration, Arizona State University, Tempe, AZ 85287, USA
[k] School of Molecular Sciences, Arizona State University, Tempe, AZ, 85287, USA

ARTICLE INFO

Article history:
Received 11 January 2019
Received in revised form 11 November 2019
Accepted 17 November 2019
Available online xxxx
Editor: I. Halevy

Keywords:
Devonian-Carboniferous
mass extinction
Hangenberg Crisis
marine anoxia
uranium isotopes
biogeochemical model

ABSTRACT

The global Hangenberg Crisis near the Devonian-Carboniferous boundary (DCB) represents one of the major Phanerozoic mass extinction events, which shaped the roots of modern vertebrate biodiversity. Marine anoxia has been cited as the proximate kill mechanism for this event. However, the detailed timing, duration, and extent of global marine redox chemistry changes across this critical interval remain controversial because most of the studies to date only constrain changes in local or regional redox chemistry. Thus, opinions on the significance of anoxia as a kill mechanism are variable—from anoxia being a primary driver to being relatively unimportant. In this study, we explore the evolution of global marine redox chemistry using U isotopes of marine limestones. The $\delta^{238}U$ trends at Long'an section in South China document systematic oscillations with three negative shifts punctuated by two positive events in between. The magnitude of the $\delta^{238}U$ oscillations implies that the sediments do not record contemporaneous seawater with a constant offset at all times. The lack of covariation between $\delta^{238}U$ data and diagenetic indicators (e.g., Mn and Sr contents, Mn/Sr ratio, $\delta^{18}O$) suggests that the $\delta^{238}U$ trends are not produced by the same post-depositional diagenetic processes. Instead, trace-metal enrichments suggest that more reducing conditions prevailed during the deposition of the two positive events. We present plausible model scenarios that fit the observed $\delta^{238}U$ trends in the context of redox-sensitive trace metal data suggesting marine anoxia expanded in the latest Devonian oceans to cover >5% of the continental shelf seafloor area. The rapid expansion of marine anoxia coincident with the onset of the Hangenberg Crisis supports marine anoxia as an important kill mechanism. Biogeochemical modeling of the coupled C-P-U cycles suggests that intensified continental weathering, for example, assisted by the spread of seed plants with deeper root systems at this time, could have triggered expansion of marine anoxia and other global changes (e.g., positive excursion in $\delta^{13}C_{carb}$ and decrease in sea surface temperature) in the latest Devonian. The anoxic event is inferred to have been transient as climatic cooling would have reduced weathering fluxes.

* Corresponding author at: School of Earth Sciences and Engineering, Nanjing University, 163 Xianlin Avenue, Nanjing 210023, China.
E-mail addresses: fzhang@nju.edu.cn, zhff414@hotmail.com (F. Zhang).

https://doi.org/10.1016/j.epsl.2019.115976
0012-821X/

1. Introduction

The Late Devonian mass extinction, which occurred in two main phases between 375 and 359 Ma, is one of the "Big Five" mass extinctions in Earth history, marked by a 70–82% extinction rate among marine invertebrate species (Sallan and Coates, 2010). The Late Devonian mass extinction comprised a series of extinction pulses. The main crises occurred at the Frasnian-Famennian stage boundary (~374 Ma) and during the Hangenberg Event close to the Devonian-Carboniferous transition (~359 Ma) (Sallan and Coates, 2010; Becker et al., 2012; Kaiser et al., 2016). Various causes for these extinctions have been proposed, including volcanism, climate change, sea-level changes, global cooling, submarine hydrothermal activity, and/or expansion of marine anoxia/euxinia (e.g., Joachimski and Buggisch, 2002; Tribovillard et al., 2004; Joachimski et al., 2009; White et al., 2018).

Recent work has provided new insights into environmental changes associated with the latest Devonian Hangenberg extinction. Widespread marine anoxia at that time is recorded by globally extensive black, organic-rich mudrock deposition (Algeo et al., 1995; Caplan and Bustin, 1999; Marynowski and Filipiak, 2007; Marynowski et al., 2012; Becker et al., 2016; Kaiser et al., 2016). High-resolution chemostratigraphic studies have provided detailed records of environmental changes in specific regions. In deep-water black shales of central Poland, there is evidence for the development of photic-zone euxinia from green-sulfur bacterial biomarkers (Marynowski and Filipiak, 2007) as well as pyrite framboid size distributions and significant trace metal evidence (Marynowski et al., 2012). In shallow-marine carbonate sections in South China, bulk nitrogen isotope variations suggest locally enhanced nitrogen fixation, possibly as a consequence of increased denitrification in response to expanded marine anoxia (Liu et al., 2016), and I/Ca ratios suggest expansion of the oxygen minimum zone into the ocean-surface layer (Liu et al., 2019). There is abundant evidence for redox shifts during the latest Devonian, but all previous studies focused on local or regional redox chemistry changes—in many cases from semi-isolated settings. Therefore, the secular evolution of global marine redox conditions during the latest Devonian remains poorly constrained, despite its importance for understanding global cause-and-effect relationships during the Hangenberg extinction event.

To fill this gap, we investigated the uranium isotope composition of marine limestones (denoted as $\delta^{238}U$), a proxy that can be used to place quantitative constraints on global marine redox chemistry changes (e.g., Dahl et al., 2014; Lau et al., 2016; 2017; Clarkson et al., 2018; Zhang et al., 2018a; 2018b; 2018c; White et al., 2018; Zhang et al., 2019a; 2019b), in the Long'an section, South China, which captured the Hangenberg extinction event. We then used a global uranium cycle model to explore the timing, duration, and extent of global marine redox changes during the Hangenberg extinction event. Finally, we used a global model of C-P-U cycling to test the hypothesis that the spread of seed plants and an associated increased P release could have triggered this event.

2. Geological background

The Long'an section is located on the South China Craton, which was situated in the eastern Tethys Ocean close to the equator during the Devonian-Carboniferous transition (Fig. 1). At that time, the southern (paleo-eastern) margin of the South China Craton consisted of a large marine embayment, comprising many shallow carbonate platforms (the Xianggui-Qiangui platform complex) and deep-water troughs of which the Youjiang Basin was the largest. The proximal platforms were attached to the southern margin of the South China Craton, whereas the distal platforms were isolated from land areas by intervening troughs.

The Long'an section is located in Dujie Village of Long'an County in Guangxi Zhuang Autonomous Region (23°10'34.8″ N; 107°27'48.0″ E). The litho- and biostratigraphy of the study section were described in detail by Qie et al. (2015) and Liu et al. (2016). Briefly, the 38-m-thick Long'an section is divided into the Yonghsien and Long'an formations (Fig. 2). The Yonghsien Formation (−30 to 0 m) consists mainly of massive bioclastic wackestone, packstone, and grainstone, whereas the Long'an Formation (0 to 8 m) is dominated by thin-bedded calcisphere wackestone and packstone. The D–C boundary, which is defined by the first appearance of the conodont *Siphonodella sulcata* (a linear descendant of *S. praesulcata*) is located at ~6 m above the base of the Long'an Formation, and the base of the Upper *praesulcata* and Middle *praesulcata* zones are located at ~2 m and ~3.3 m below the base of the Long'an Formation, respectively (Qie et al., 2015; Liu et al., 2016). Sedimentological evidence (i.e., presence of bioturbation) indicates that the entire study interval was deposited in an oxic shallow-marine setting (Qie et al., 2015), consistent with the study units being passive recorders of seawater U isotope composition with an offset similar to that in modern Bahamian carbonate sediments (Romaniello et al., 2013; Chen et al., 2018).

In this study, 55 nearly pure limestone samples ($CaCO_3$ content from 92.7% to 99.9% with a mean of 98.5%; see Liu et al., 2016)

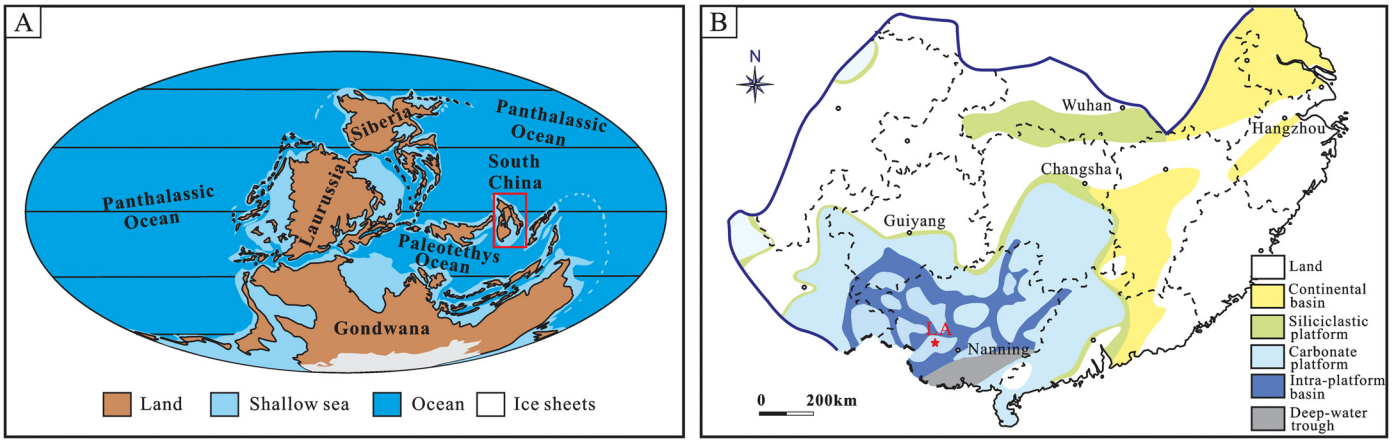

Fig. 1. Late Devonian paleogeography. (A) Global paleogeography (modified from Scotese and McKerrow, 1990). The red rectangle represents the area of map B. (B) South China paleogeography (modified from Qie et al., 2015). Study locale is shown by star: LA: Long'an. (For interpretation of the colors in the figure(s), the reader is referred to the web version of this article.)

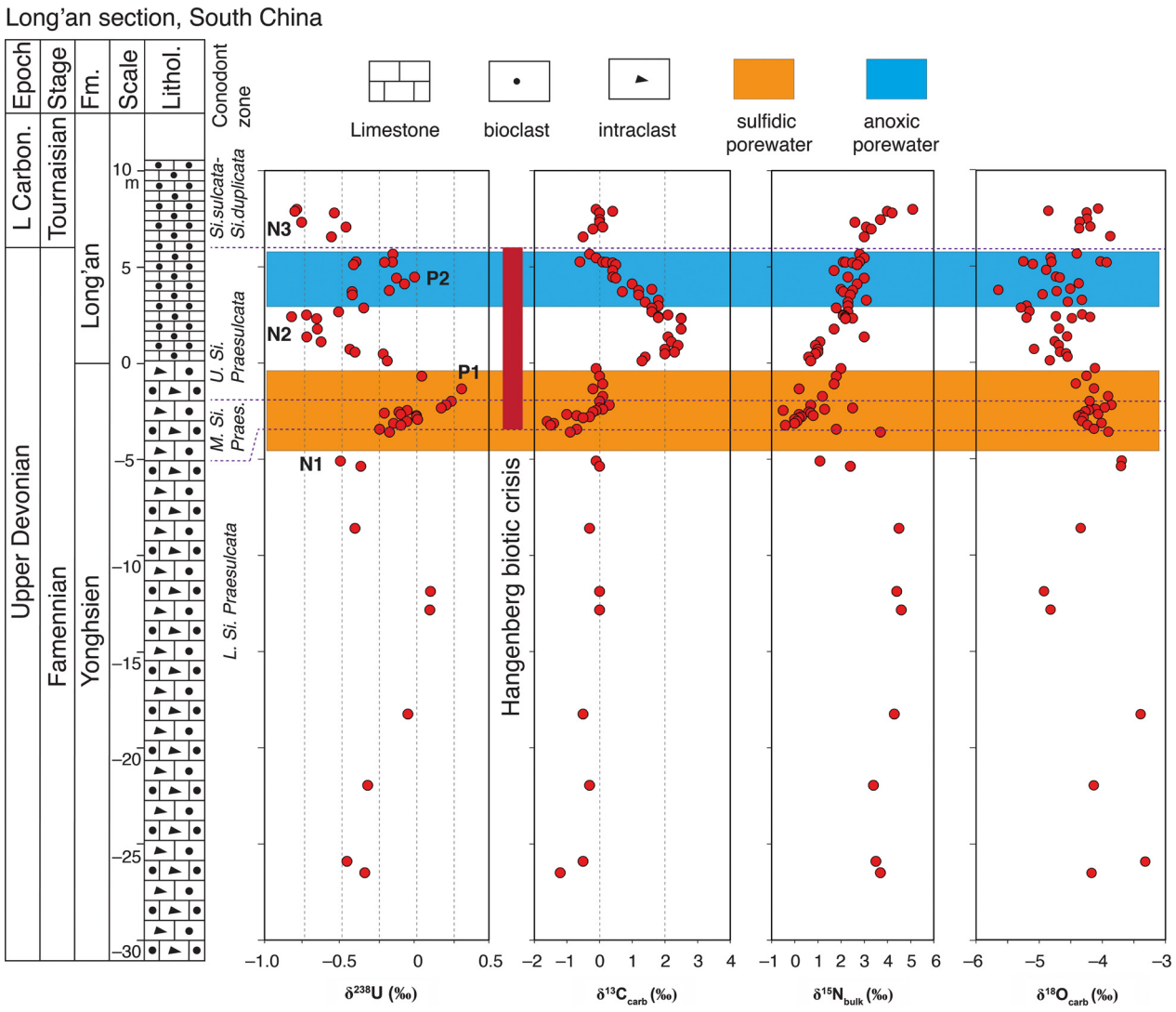

Fig. 2. $\delta^{238}U$, $\delta^{13}C_{carb}$, and $\delta^{15}N_{bulk}$ profiles of Long'an section in South China. L Carbon., Lower Carboniferous; Fm., Formation; Lithol., Lithology. P1 and P2 denote positive $\delta^{238}U$ excursions, and N1, N2, and N3 denote negative $\delta^{238}U$ excursions.

were analyzed for $\delta^{238}U$ and major and trace elements. $\delta^{13}C_{carb}$, $\delta^{15}N_{bulk}$, and I/Ca ratio data from the same suite of samples have been previously reported by Qie et al. (2015), Liu et al. (2016), and Liu et al. (2019).

3. Analytical methods

Three to five grams of carbonate powder were dissolved in 1 M hydrochloric acid (HCl) for 24 h at room temperature. Digests were centrifuged and the supernatant was separated. A split of each supernatant was diluted to ~200 ppm calcium (Ca) with 2% HNO_3 and analyzed for a full suite of major and trace element concentrations on a Thermo iCAP quadrupole inductively coupled plasma mass spectrometer (Q-ICP-MS) at the W. M. Keck Laboratory for Environmental Biogeochemistry at Arizona State University (ASU). Typical precision was better than 3% and 5% for major and trace elements, respectively, based on repeated analysis of in-run standards.

Prior to U purification by ion exchange chromatography, appropriate amounts of ^{236}U:^{233}U double spike (e.g., Romaniello et al., 2013; Zhang et al., 2018a; 2018b; 2018c; Chen et al., 2018; Zhang et al., 2019a; 2019b) were added to each sample to correct for instrumental and procedural mass-dependent fractionation of the measured $^{238}U/^{235}U$ ratio. The spike-sample mixtures were evaporated to dryness and taken up in 3 N HNO_3. Uranium was purified using the UTEVA method (e.g., Romaniello et al., 2013; Chen et al., 2018; Zhang et al., 2018a; 2018b; 2018c; White et al., 2018 for details) before isotopic analysis. All samples were put through UTEVA resin twice in order to completely remove matrix ions. The final purified U was dissolved in 0.32 M HNO_3 and diluted to a U concentration of 50 ppb. Uranium isotopes were measured at ASU on a Thermo-Finnigan Neptune multi-collector ICP-MS at low mass resolution. The standard solution CRM145 (50 ppb U) was analyzed every two samples. Two secondary standards CRM129a and Ricca ICP solution were measured after every fifteen measurements. Sample $\delta^{238}U$ values were normalized by the average of the bracketing standards. The $\delta^{238}U$ results are summarized in Fig. 2 in the main text and in the *Supplementary Data* file.

4. Results

$\delta^{238}U$ values at the Long'an section range from −0.82‰ to +0.32‰ (see Fig. 2 and *Supplementary Data* file). The $\delta^{238}U$ data display a coherent curve with three negative excursions (N1 to N3) separated by two positive excursions (P1 and P2; Fig. 2). The N1 event (a ~0.6‰ negative shift) began in the uppermost Lower *Siphonodella praesulcata* Zone and ended in the lower Middle *S. praesulcata* Zone. The N2 event (a ~1.0‰ negative shift) began in

the lower Upper *S. praesulcata* Zone and ended in the upper Upper *S. praesulcata* Zone. The N3 event (a ~0.8‰ negative shift) began in the uppermost Upper *S. praesulcata* Zone and ended in the lower *S. sulcata-S. duplicata* zones. Using the measured thicknesses of conodont biozones at Long'an (Qie et al., 2015; Liu et al., 2016; 2019) and the radiometric Devonian time scale of Becker et al. (2012), in which the duration of each conodont zone was calibrated, we calculated an average sedimentation rate of ~37 m/Myr and a total duration of ~1 Myr for the study interval. We are not implying perfectly linear sedimentation, but a total duration of ~1 Myr is supported by a robust biostratigraphic framework.

5. Discussion

5.1. Evaluation of post-depositional alteration of $\delta^{238}U$ signals in the Long'an section

The carbonate U isotope redox proxy is a relatively new proxy compared to traditional carbonate C, O, and Sr isotope systematics. Modern carbonate samples from the Bahamas yield ^{238}U values with an offset range from 0 to 0.5‰ with an average of 0.27±0.14‰ (1 SD) relative to the overlying seawater (Romaniello et al., 2013; Chen et al., 2018). This offset is generated syndepositionally close to the sediment-water interface (Romaniello et al., 2013). This is a common feature in carbonate sediments, although the redox states of the sediment porewater played an important role (Romaniello et al., 2013), there is still some uncertainty about the processes governing the magnitude of this offset. Samples with evidence for more open-system diagenetic exchange (low Sr/Ca, high Mn/Sr) have been shown to yield slightly greater offsets Dahl et al. (2019). However, diagenetic modeling suggests that preservation of carbonate $\delta^{238}U$ signals should be substantially more robust during fluid exchange than $\delta^{18}O$ and $^{87}Sr/^{86}Sr$ (Lau et al., 2017; Chen et al., 2018), and comparisons of deep drill core samples further confirm that $\delta^{238}U$ is not affected to the same degree as $\delta^{13}C$ and $\delta^{18}O$ (Chen et al., 2018; Tissot et al., 2018).

In this study, we evaluated potential diagenetic alteration using conventional geochemical criteria. Low Mn contents, high Sr contents, low Mn/Sr ratios, and relatively high $\delta^{18}O$ values are characteristic of carbonate sediments with minimal influence by meteoric diagenesis (e.g., Banner and Hanson, 1990; Jacobsen and Kaufman, 1999; Lau et al., 2016; White et al., 2018; Zhang et al., 2019a). In the Long'an section, Mn contents vary from 11.5 ppm to 90 ppm with a mean of 35 ppm, Sr contents vary from 168 ppm to 557 ppm with a mean of 310 ppm, and Mn/Sr ratios vary from 0.03 to 0.33 with a mean of 0.12. These characteristics are consistent with well-preserved marine carbonates with minimal chemical alteration during burial diagenesis (e.g., Banner and Hanson, 1990; Jacobsen and Kaufman, 1999; Lau et al., 2016; White et al., 2018; Zhang et al., 2019a; Fig. S1 in the supplementary material). This hypothesis is further supported by O isotope data ($\delta^{18}O$ values > −6‰), which are within the typical range of best preserved Phanerozoic marine carbonate $\delta^{18}O$ values (e.g., Veizer et al., 1999). Therefore, we infer that interaction with meteoric or burial fluids is unlikely to have significantly altered the $\delta^{238}U$ record at Long'an.

Changes in lithology—such as dolomitization—are not a concern in the study section. The Mg/Ca molar ratios in the samples are well below 0.01, suggesting negligible dolomitization. Other changes in mineralogy—such as the transformation of aragonite to calcite—can release U into pore fluids. This transformation, however, generally occurs at greater burial depths at which insoluble U(IV) is stable and, thus, any U isotope fractionation in the limestones will be muted or not expressed (Henderson et al., 1999; Romaniello et al., 2013; Chen et al., 2016; Chen et al., 2018). Further, there is no relationship to bulk carbonate Sr/Ca ratios, which are sensitive to aragonite dissolution and Sr capture in secondary calcite phases, which suggests a limited influence from aragonite-to-calcite transition on observed $\delta^{238}U$ trends.

Contamination from detrital materials is also not a concern for $\delta^{238}U$ in the study section. Dissolution of carbonate sediments using 1 M HCl has the potential to liberate U from detrital materials. We evaluated this possibility based on Al concentrations and U/Al ratios. Aluminium concentrations range from 8 ppm to 133 ppm with a mean of 39 ppm, confirming that the study samples are relatively pure carbonates with low detrital content. U/Al ratios, which range from 28 to 4114 ppm/wt.%, are significantly higher than the average upper continental crustal value of 0.33 ppm/wt.% (Rudnick and Gao, 2014) or the topsoil mean value of 0.58 ± 1.13 ppm/wt.% (Cole et al., 2017), indicating that our sample digestion protocol has effectively extracted carbonate-associated U. Even if some detrital U was extracted, it is quantitatively insignificant and does not affect the reported $\delta^{238}U$ values.

Although the analysis above indicates that Long'an carbonates were not strongly altered by post-depositional diagenetic processes, the P1 interval is nonetheless enriched in Fe, Zn, Mo, and U (Fig. 3), suggesting that it was influenced by sulfidic pore fluids in the early diagenetic environment and/or by an input of dissolved metals to the global oceans due to changes in terrestrial weathering. Fe, Zn, and Mo are redox-sensitive chalcophile metals that accumulate in sediments in which dissolved H_2S is present in pore fluids (Tribovillard et al., 2006). During expansion of marine anoxia, rapid reduction of seawater-soluble U(VI) can lead to massive accumulation of insoluble and isotopically heavier U(IV) below the sediment-water interface. With dissolved H_2S present in sediment pore fluids, isotopically heavy U(IV) can be incorporated into carbonate precipitates. This process has been well documented on the modern Bahamian carbonate platform (Romaniello et al., 2013). Although the overlying water column is well oxygenated, Bahamian sediment pore-waters become sulfidic ~5 cm below the sediment-water interface as a result of abundant organic matter and high rates of respiration and sulfate reduction (Romaniello et al., 2013). We acknowledge that Fe, Zn, and Mo concentrations in carbonates can be biased by the incorporation of terrestrial Fe, Zn, and Mo contributions (i.e., in association with an episode of enhanced terrestrial weathering input). This possibility during the P1 event can, however, be ruled out by the Al normalized elemental plots (Fe/Al, Zn/Al, and Mo/Al; Fig. 3) where stratigraphic spikes in Fe, Mo, and Zn are retained and, therefore, argue for authigenic Fe, Mo, and Zn enrichments during the P1 event. Building from these observations, we suggest that the pronounced U enrichments and the high $\delta^{238}U$ values of the P1 event were most likely a product of strongly reducing pore-water conditions that induced significant authigenic U(IV) enrichments and thus a larger-than-usual early diagenetic offset. This hypothesis has been further modeled in section 5.3. Our study is limited to one section, and we encourage further studies of other sections to assist in disentangling local from global U isotope signals.

In contrast to the P1 event, the P2 event exhibits only Fe and Zn enrichments but no Mo enrichments, although U concentrations are still enriched relative to adjacent sediments. The spikes in Fe and Zn during the P2 event, however, disappears when normalized to Al concentrations (Fig. 3), suggesting that these spikes are mainly associated with a terrestrial input of dissolved metals to the latest Devonian oceans and not driven by local Fe and Zn sulfide precipitation in sulfidic porewaters. Given the fact that Fe, Zn, and Mo sequestration in sediments is strongly enhanced by the presence of free H_2S, reductive immobilization of U is less sensitive to H_2S (Tribovillard et al., 2006), the lack of Fe/Al, Zn/Al, and Mo/Al spikes within the P2 interval could indicate anoxic and non-sulfidic pore-water conditions, which led only to small U enrichments (see section 5.3 for further model interpretations). We, however, could

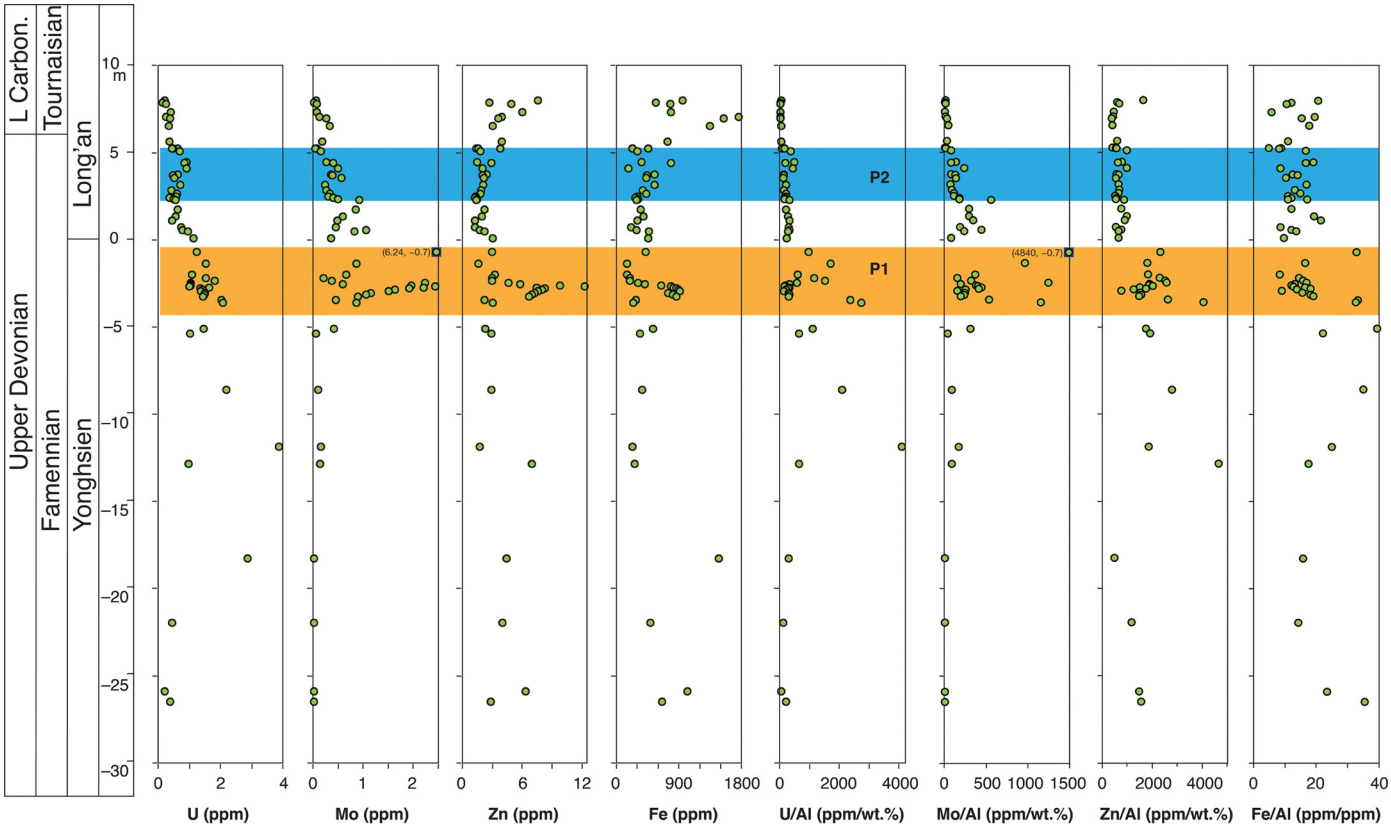

Fig. 3. Trace element profiles and elemental ratios of Long'an section. The orange/blue shaded area denotes horizons affected by sulfidic/anoxic pore-water conditions.

not fully rule out the possibility that the P2 event represented a global ocean reoxygenation event; this possibility has been modeled in section 5.4 using a C-P-U model, and distinguish between models in section 5.3 and 5.4 requires δ^{238}U measurements from another section.

In the modern Bahamas, both bank-top and deep-slope carbonates have δ^{238}U compositions that are heavier than that of contemporaneous seawater by 0–0.5‰ (average of 0.27±0.14‰, 1SD). This offset is not constant and has been attributed to incorporation of ^{238}U-enriched U(IV) from anoxic pore waters during early diagenesis (Romaniello et al., 2013) or variations in pore-water U-speciation during carbonate recrystallization (Chen et al., 2018). The influence of syndepositional processes on carbonate U are possible because shallow, relatively permeable carbonates can sequester dissolved U(VI) from the overlying oxic water column via advective and diffusive transport. This semi-open system behavior allows an exchange of U isotopes that can induce a net ^{238}U offset in bulk carbonate sediments relative to primary carbonate phases. As stated above, this process is not significant at greater burial depths because the mobility of U is severely restricted in anoxic pore fluids, as shown by nearly identical δ^{238}U offsets in Bahamian carbonates regardless of mineralogy (e.g., aragonite, low-Mg calcite, or dolomite), water depth, and depth below the sediment-water interface (Chen et al., 2018; Tissot et al., 2018). On this basis, we have applied a diagenetic correction factor to measured δ^{238}U values prior to the U isotope mass balance calculations presented below.

5.2. Quantifying marine redox changes using a uranium isotope mass balance model

In order to quantitatively estimate the duration and extent of marine redox variations, we used the U isotope mass balance model of Zhang et al. (2019a) (see also Lau et al., 2016) to calculate the proportion of total marine U burial in anoxic sediments (f_{anoxic}) and to estimate the areal extent of marine anoxia in latest Devonian oceans (A_{anoxic}).

The implied changes to the extent of marine anoxia can be described by differential mass balance equations for the seawater U reservoir and its source and sink fluxes:

$$\frac{dN_{sw}}{dt} = J_{river} - J_{anoxic} - J_{other} \quad (1)$$

$$\frac{d(N_{sw} \cdot \delta^{238}U_{sw})}{dt} = J_{river} \cdot \delta^{238}U_{river} - J_{anoxic} \cdot \delta^{238}U_{anoxic} - J_{other} \cdot \delta^{238}U_{other} \quad (2)$$

$$\delta^{238}U_{anoxic} = \delta^{238}U_{sw} + \Delta_{anoxic} \quad (3)$$

$$\delta^{238}U_{other} = \delta^{238}U_{sw} + \Delta_{other} \quad (4)$$

Eq. (2) can be rewritten as:

$$\frac{d(N_{sw} \cdot \delta^{238}U_{sw})}{dt} = J_{river} \cdot \delta^{238}U_{river} - J_{anoxic} \cdot (\delta^{238}U_{sw} + \Delta_{anoxic}) - J_{other} \cdot (\delta^{238}U_{sw} + \Delta_{other}) \quad (5)$$

where N_{sw} is the oceanic uranium inventory in moles, $\delta^{238}U_{sw}$, $\delta^{238}U_{river}$, $\delta^{238}U_{anoxic}$, and $\delta^{238}U_{other}$ are the U isotope compositions of seawater, riverine sources, anoxic sedimentary sinks, and the average of the remaining other sinks, respectively. J_{river} is the riverine U flux in mol/yr. A Δ_{anoxic}= +0.6‰ is the average isotopic difference between anoxic/euxinic sediments and contemporaneous seawater (e.g., Andersen et al., 2014), and Δ_{other} is the average isotopic difference between contemporaneous seawater and the remaining other sinks (~ +0.05 ‰, calculated to maintain an isotopic steady state in the modern ocean).

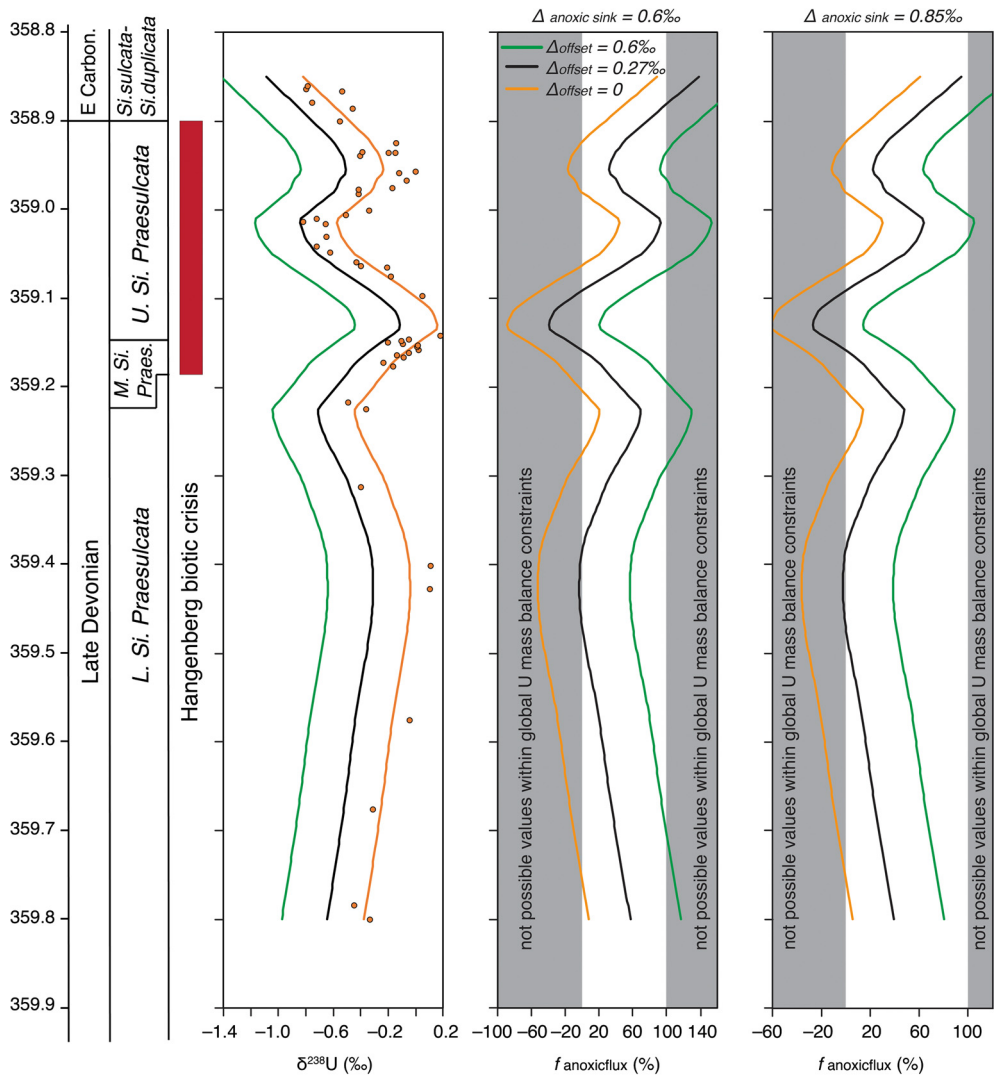

Fig. 4. Mass balance calculations of fraction of uranium removal to anoxic sinks based on diagenetic offsets (Δ_{offset}) of 0‰, 0.27‰, and 0.3‰. Two independent calculations using fractionation factors between seawater and anoxic sinks of 0.6‰ and 0.85‰, respectively, are shown for comparison.

Following prior studies (e.g., Dahl et al., 2014; Lau et al., 2016; 2017; Zhang et al., 2018b, 2019a), we define J_{anoxic} as:

$$J_{anoxic} = A_{anoxic} \cdot k_{anoxic} \cdot N_{sw} \quad (6)$$

where A_{anoxic} is the total seafloor area overlain by anoxic waters and k_{anoxic} is the rate constant associated with anoxic sediment deposition. Solving equations (1) and (2) at a steady state, we have:

$$f_{anoxic} = \frac{\delta^{238}U_{river} - \delta^{238}U_{sw} - \Delta_{other}}{\Delta_{anoxic} - \Delta_{other}} \quad (7)$$

where $f_{anoxic} = J_{anoxic}/J_{river}$, and the $\delta^{238}U_{SW}$ of the latest Devonian oceans can be estimated using observed $\delta^{238}U$ data for Long'an minus the early diagenetic offset (Δ_{offset}, the $\delta^{238}U$ difference between carbonate sediments and overlying seawater):

$$\delta^{238}U_{sw} = \delta^{238}U_{carb} - \Delta_{offset} \quad (8)$$

Measured carbonate $\delta^{238}U$ for Long'an spans a wide range of values up to +0.2‰. These high values are beyond what can be achieved in open-ocean seawater (where $\delta^{238}U_{sw} < -0.28‰ = \delta^{238}U_{river}$; e.g., Andersen et al., 2017), and therefore these carbonates record seawater with a substantial offset ($\delta^{238}U_{carb} - \delta^{238}U_{sw} = \Delta_{offset}$). A positive Δ_{offset} is consistent with that observed in drill cores from the modern Bahamian platform (i.e., Δ_{offset} ranges from 0 to 0.5‰ with an average of $+0.27 \pm 0.14$‰, 1 SD; Chen et al., 2018; Tissot et al., 2018). Larger Δ_{offset} up to +0.6‰ are known to occur in reducing sediments with substantial authigenic U(IV) enrichments (e.g., core 1 from the *T. testudium* flat in the Bahamas; Romaniello et al., 2013). The relatively high $\delta^{238}U$ values in the P1 and P2 intervals imply higher Δ_{offset} values at those times (i.e., due to anoxic/sulfidic porewater conditions discussed in section 5.1), and these intervals are also characterized by greater U enrichments than other intervals of the Long'an section.

To show that the ocean oxygenation state varied both at the global scale and in the Long'an basin, we first calculated steady state f_{anoxic} values from Eqs. (7) and (8) assuming constant values for Δ_{offset} of 0‰, +0.27‰, and +0.6‰ (Fig. 4). The other model parameters are given in Table 1. In order to avoid overinterpretation of noise in the $\delta^{238}U_{carb}$ dataset, we interpolated and smoothed measured $\delta^{238}U_{carb}$ values using a LOWESS (LOcally WEighted Scatterplot Smoothing) fit method with a span parameter equal to 0.4. The isotope-driven calculation of f_{anoxic} values shows that the U burial flux into anoxic sediments was significantly greater during the N1, N2, and N3 intervals than today.

All three curves (based on Δ_{offset} of 0‰, +0.27‰, and +0.6‰) show f_{anoxic} values that are not possible within global U mass balance constraints for some time intervals (i.e., intervals with high

Table 1
Uranium box model parameterization.

Model parameters		Modern		Reference
Ocean volume	V_{ocean}	1.30E+21	L	
Oceanic U inventory	N_{sw}	1.90E+13	mol	
Anoxic seafloor area	A_{anoxic}	0.5%	(% of total seafloor)	
Fluxes				
Oceanic input flux (rivers, groundwater, aeolian)	J_{river}	5.30E+7	mol/yr	Dunk et al., 2002
Sediment burial flux in anoxic settings	J_{anoxic}	1.17E+7	mol/yr	Dunk et al., 2002
Sediment burial flux in other settings	J_{other}	4.64E+7	mol/yr	Dunk et al., 2002
Uranium isotope cycle				
Uranium isotope composition of oceanic input	$\delta^{238}U_{river}$	−0.27	‰	Andersen et al., 2017
Uranium isotope difference between buried anoxic sediments and seawater	$\Delta^{238}U_{anoxic}$	+0.60	‰	Andersen et al., 2017
Uranium isotope difference between buried other sediments and seawater	$\Delta^{238}U_{other}$	+0.05	‰	Dahl et al., 2014
Uranium isotope difference between carbonates and seawater	$\Delta^{238}U_{carb}$	+0.24	‰	Chen et al., 2018
Maximal U isotope offset in carbonates	$\Delta_{offset,\,maz}$	+0.60	‰	Romaniello et al., 2013
Local conditions at Long'an	Δ_{offset}	change with time	‰	

$\delta^{238}U_{carb}$ values such as P1 and P2 events; Fig. 4), suggesting that the Δ_{offset} was not constant and must have varied temporally during accumulation of the Long'an carbonates. We model this possibility by simultaneously changing A_{anoxic} and Δ_{offset} in Equations (5), (7) and (8) to generate the $\delta^{238}U_{carb}$ trend observed in the Long'an section. Although this approach gives a range of f_{anoxic} solutions for the Long'an dataset, we can nonetheless draw certain conclusions about the solution space. We provided two distinct model scenarios to explain the observed $\delta^{238}U_{carb}$ trend of the Long'an section (Fig. 5) that allow higher Δ_{offset} values at P1 and P2 where elevated Mo and/or U enrichments indicate more reducing pore-water conditions in the early diagenetic environment (Figs. 3 and 5).

The first modeled scenario (Fig. 5, model scenario 1) started from an oxygenated ocean similar to that of the modern, with the onset of anoxic expansion at the peak of P1 (~359.1 Ma). The second scenario (Fig. 5, model scenario 2) started from the same baseline as the first scenario but incorporated an earlier expansion of anoxia (~359.2 Ma) where the U concentration begins to drop. The first modeled scenario fits the $\delta^{238}U_{carb}$ trend of Long'an better, and it also produces a distribution of Δ_{offset} similar to that observed in modern Bahamian carbonates (Fig. 6), but it fails to mirror the observed U concentration profile. In contrast, the second modeled scenario fits the observed U concentration trend better, but it cannot fully fit the peak of the $\delta^{238}U_{carb}$ trend at P1 because Δ_{offset} becomes larger than for modern carbonates but is limited to 0.6‰ in our model (Fig. 6). $\delta^{238}U$ offset distribution test supports that our modelled seawater $\delta^{238}U$ curve is realistic, but it does not rule out other plausible seawater $\delta^{238}U$ curves. This will not be resolved until new $\delta^{238}U_{carb}$ curves are generated at other sections. Nevertheless, both model scenarios suggest that global marine anoxia expanded significantly, covering >5% of continental shelf areas in the latest Devonian oceans. The maximal extent of marine anoxia is difficult to constrain because modeled $\delta^{238}U$ is insensitive to expanding anoxia once the anoxic U sink dominates other U sink fluxes. However, a >5% expansion of anoxic marine zones is large enough to have extended over most continental shelf areas, which account for just 7.6% of total seafloor area in the modern ocean. The expansion of marine anoxia was coincident with the onset of the Hangenberg Crisis at the base of the Middle *Siphonodella praesulcata* Zone (Fig. 5). The modelled f_{anoxic} curves in Fig. 5 are consistent with the observation that U concentrations overall decrease across the anoxic event in tandem with the changes in I/Ca and nitrogen isotopes (Liu et al., 2016, 2019). A full recovery to the pre-expansion background state is, however, not recorded in the studied Long'an section.

Both model scenarios can explain the observed P1 and P2 events at the Long'an section by invoking redox changes in the sediment pore-water environment. According to the model, these positive events can be reasonably explained by intensified anoxic/sulfidic conditions in the sediment pore fluids (or in theory the water column above the water-sediment interface based on I/Ca and $\delta^{15}N$ evidence from the Long'an section; Liu et al., 2016, 2019), which precipitated ^{238}U-enriched U(IV) into the Long'an carbonates during the P1 and P2 intervals. For example, our model shows that Δ_{offset} values must have approached +0.6‰ in the P1 interval and +0.4 to +0.6‰ in the P2 interval (Fig. 5).

Our $\delta^{238}U$ data, along with biomarker and other evidence for widespread oceanic anoxia elsewhere globally Algeo et al. (1995); Caplan and Bustin (1999); Marynowski and Filipiak (2007); Marynowski et al. (2012); Liu et al. (2016, 2019), confirm that a large proportion of latest Devonian outer continental shelves and upper slopes were covered by anoxic waters. The expansion of marine anoxia would have promoted extensive black, organic-rich mudrock deposition (Algeo et al., 1995; Caplan and Bustin, 1999) and allowed the buildup of H_2S in shallow-water environments (Marynowski and Filipiak, 2007; Marynowski et al., 2012). It also increased sediment burial of reduced carbon and sulfur relative to oxidized forms, leading to large positive shifts in $\delta^{13}C_{carb}$ and $\delta^{34}S_{CAS}$ globally (Brand et al., 2004; Kaiser et al., 2006; 2008; Qie et al., 2015; Liu et al., 2016).

5.3. Testing links of marine anoxia to the spread of land plants and enhanced chemical weathering

The Late Devonian was a key interval in the evolutionary history of land plants, as the appearance of the earliest seed plants allowed the spread of terrestrial vegetation into upland areas for the first time (Algeo et al., 1995; Berner and Caldeira, 1997; Algeo and Scheckler, 1998). This event is thought to have resulted in a decrease of atmospheric CO_2 levels and a longer-term increase of atmospheric O_2 levels as well as to have had a deep influence on marine biogeochemical cycles (Algeo et al., 1995; Berner, 1997; Lenton, 2001). The spread of vascular plants and an associated intensification of continental weathering has been proposed to have increased marine phosphorus levels, thus generating higher marine productivity and an expansion of marine anoxic seafloor areas in latest Devonian oceans (Algeo et al., 1995; Algeo and Scheckler, 1998). Intensified continental weathering is supported by an increase in $^{87}Sr/^{86}Sr$ from ~0.70813 to ~0.70829 during the Late Devonian (Brand et al., 2004; McArthur et al., 2012). Conodont apatite oxygen-isotope data imply a concurrent ~3°C decrease

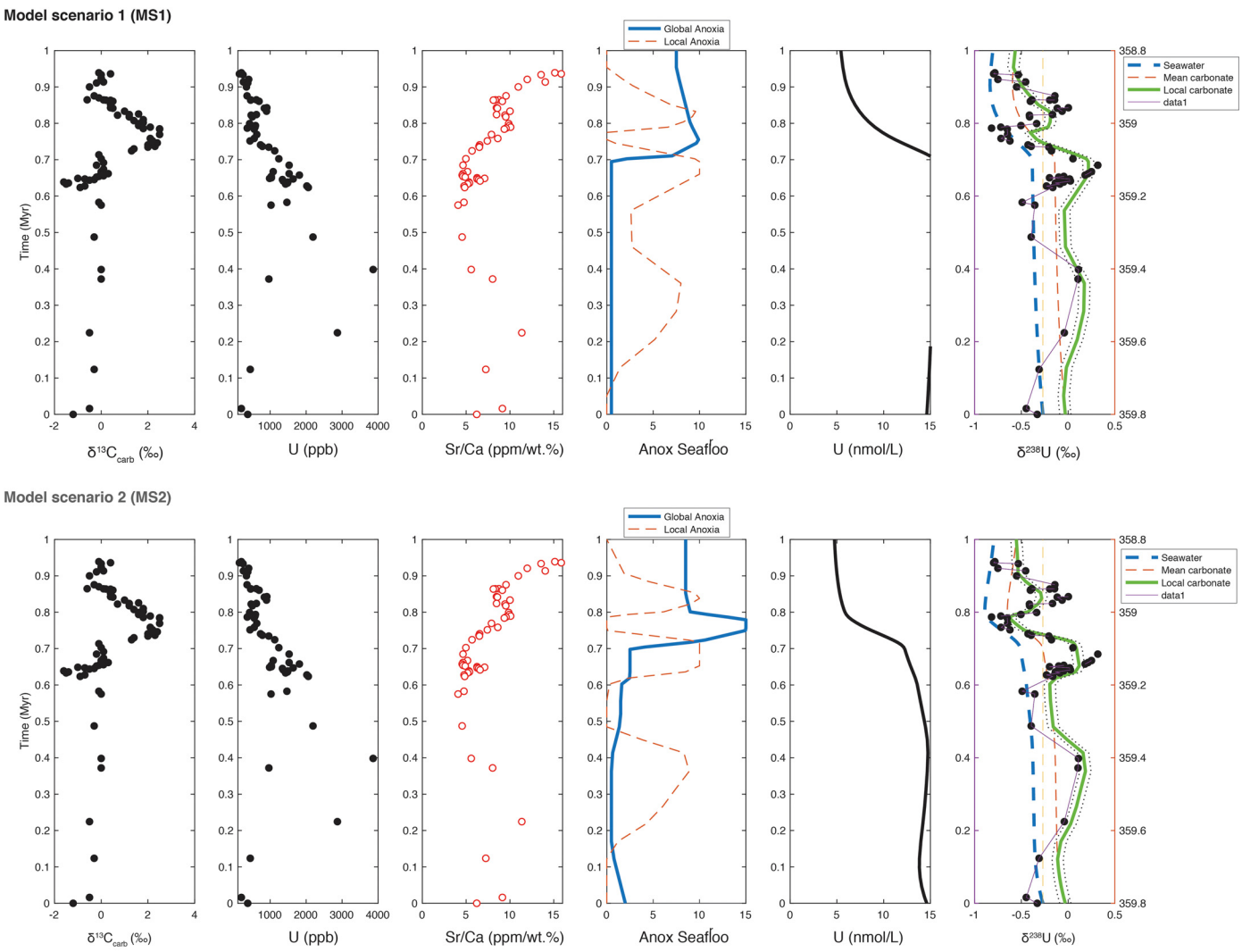

Fig. 5. U isotope model estimates of local versus global expansion of marine anoxia. In model scenario 1 (MS1), anoxic marine areas initially started from an oxygenated ocean similar to the modern-day, which started to expand at peak of P1. The local anoxia in the model is assumed to be proportional to the Δ_{offset} that can be generated between average carbonates and anoxic carbonates. The Δ_{offset} varies between 0.27‰ and 0.6‰. The model scenario 2 (MS2) started from a situation similar to that in MS1 but expanded prior to peak of P1 and further expanded between P1 and N2.

in tropical sea-surface temperatures during the latest Devonian (Joachimski et al., 2009) consistent with more intensive weathering. However, on a million-year time scale, the overall amount of silicate weathering is must be close to be in balance with carbon dioxide outgassing rates, similar to what is observed for the Cenozoic (e.g., Berner and Caldeira, 1997; Caves et al., 2016). In this light, the effect of land plants is likely to change the strength of the silicate weathering feedback or facilitate more efficient P solubilization rather to dramatically change the overall amount of silicate weathering.

To test the hypothesis that the spread of land plants caused the latest Devonian expansion of marine anoxia, we used an existing model of the coupled global C-P-U cycles (Clarkson et al., 2018), slightly updated to use the same U cycle and isotope mass balance as in Section 5.2 (see SI for full model description). We explored various plausible combinations of plant forcing factors to see under what conditions the global model could reproduce the global changes observed in the latest Devonian alongside the global component of the changes in the U isotope record.

We find that a ~33% increase in land plant cover and associated chemical weathering amplification over 200 kyr is capable of generating a transient ~–0.6‰ negative $\delta^{238}U_{sw}$ excursion, a ~2‰ positive $\delta^{13}C$ excursion, a ~3°C global cooling, and an approximate halving of CO_2 levels (Fig. 7A). The anoxic fraction of the ocean increases from 0.6% to a maximum of 11%, and the U content of the ocean declines by a factor of ~5× (Fig. 7A). By the start of the P1 event the area of marine anoxia has doubled, and at the peak of P1 it has increased 10×, consistent with our interpretation of a local anoxic signal at this time. Assuming a typical +0.27‰ offset, the initial value of $\delta^{238}U_{carb}$ reasonably matches the mean of the sparse early data (before the N1 event) and the predicted minimum of $\delta^{238}U_{carb}$, and its timing matches the N2 event well (Fig. 7B, green line). Assuming a +0.6‰ offset (blue line), an upper limit on local $\delta^{238}U_{carb}$ matches some but not all of the data for the P1 and P2 events. There are of course large uncertainties in the magnitude of the chemical weathering amplification terms. However, this modeling exercise suggests that reasonable changes in terrestrial realm could drive the observed marine perturbation.

The expansion of terrestrial floras during the latest Devonian triggered multiple effects that influenced contemporaneous marine environmental and global climatic conditions. First, expanding terrestrial floras is likely to have enhanced subaerial weathering of phosphorus and increased riverine P fluxes, resulting in increased marine productivity and organic carbon burial (Algeo et al., 1995; Algeo and Scheckler, 1998). The enhanced P delivery may be linked to slow release of organic P during transport of plants to the ma-

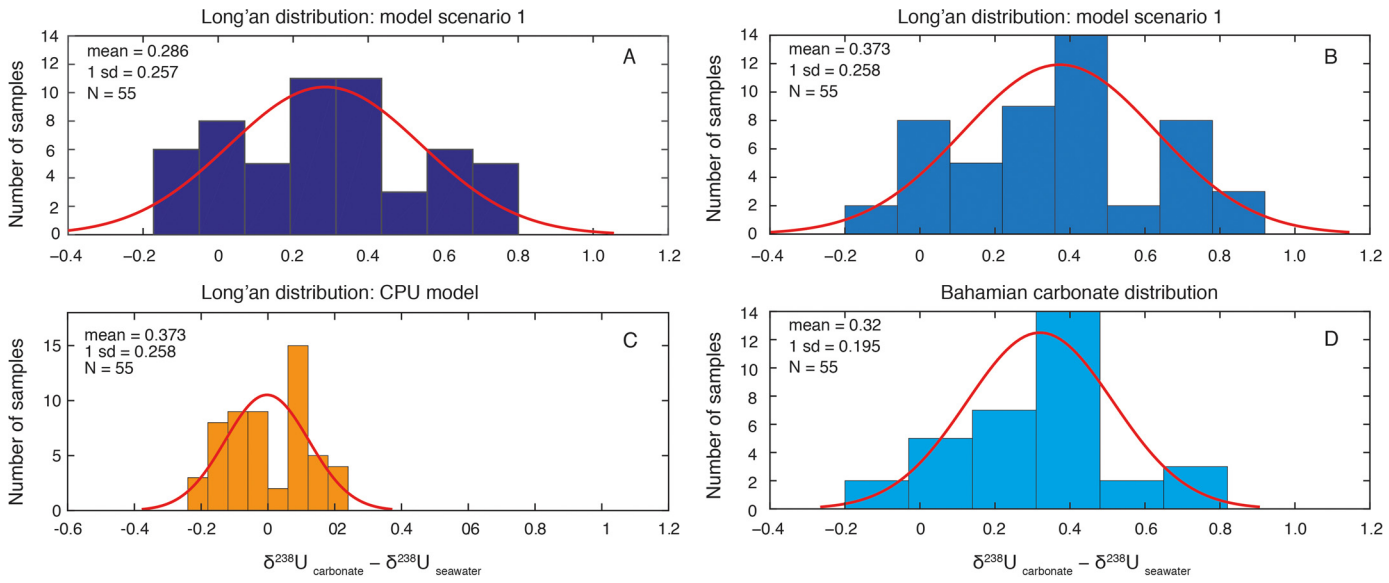

Fig. 6. Distribution of Δ_{offset} ($\delta^{238}U_{carbonate} - \delta^{238}U_{seawater}$) in model scenario 1, model scenario 2, and CPU model (Fig. 7) for Long'an compared to modern carbonates. In model scenario 1, the average Δ_{offset} is similar to that of modern carbonates but the Long'an section displays more scatter. In model scenario 2, both the average Δ_{offset} value and its variability is greater for the Long'an section than observed in modern carbonates.

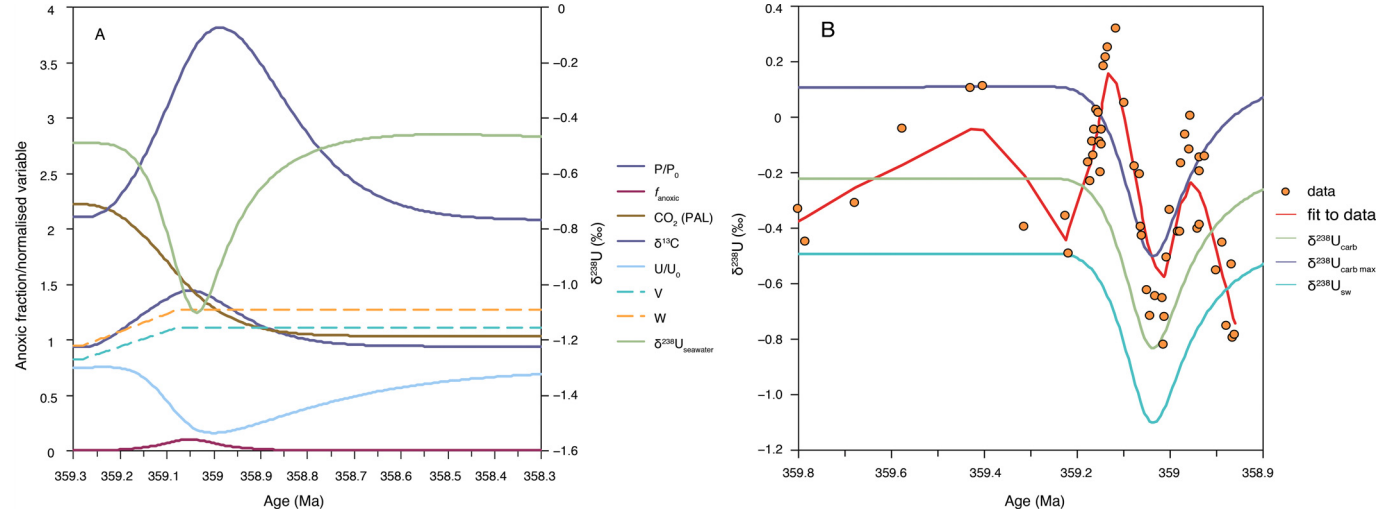

Fig. 7. Global C, P, U model scenario of increased land plant cover and enhanced continental weathering as a cause of coupled global changes. (A) Model scenario of a 33% increase in plant cover (V) and associated bulk weathering amplification (W) over 200 kyr starting at 359.28 Ma, and resulting response of normalized P content of ocean (P/P_0), anoxic fraction of ocean (f_{anoxic}), CO_2 (PAL), $\delta^{13}C$ (‰), normalized U content of ocean (U/U_0), and $\delta^{238}U_{sw}$ (‰). (B) Comparison of data (symbols), running mean of data (red line), and modelled $\delta^{238}U_{sw}$ (blue line), assuming a fixed offset (0.27‰) of $\delta^{238}U_{carb}$ from seawater $\delta^{238}U$ (green line), and maximum $\delta^{238}U_{carb}$ assuming a maximum offset of 0.6‰ from seawater (purple line). (Note the shift in the time axis between panels A and B.)

rine realm. The effects of an increased P flux to the oceans may have been amplified by enhanced phosphorus recycling from marine sediments under anoxic conditions (e.g., Ingall and Jahnke, 1994; Algeo and Ingall, 2007). Second, expanding terrestrial floras increased bulk silicate weathering in the pedosphere through production of root acids, and contributed to increased organic carbon burial through production of refractory organic matter. Collectively, these processes resulted in sharp declines in atmospheric CO_2 and temperatures during the Late Devonian (Berner, 2006; Algeo and Scheckler, 2010). However, feedbacks with the weathering-climate system tended to limit the duration of such events. For example, deep weathering of soils slowly reduces the rate of liberation of new P (Algeo and Scheckler, 1998), and release of oxygen through organic carbon burial slowly ventilates anoxic marine systems, limiting phosphorus recycling effects (Algeo and Ingall, 2007). In our model, the oceanic anoxic event (OAE) ceased after a total duration of ~400 kyr. This produced a recovery in $\delta^{238}U_{sw}$ to more positive values resembling the N2 to P2 transition, thus suggesting that the P2 event was not necessarily a local sedimentary signature.

There may have been several pulses of enhanced weathering and expansion of marine anoxia during the Late Devonian. The coupled C-P-U model with biogeochemical feedbacks (Fig. 7) predicts that a single episode of terrestrial floral expansion would have generated a transient expansion of marine anoxia. In contrast, the f_{anoxic}–Δ_{offset} models (Fig. 5) suggest that expansion of marine anoxia would have been globally more persistent. In order to generate a second expansion of marine anoxia in the C-P-U model (and match the N3 data), a second episode of terrestrial floral expansion can be invoked, but again the consequences would have been transient. Given the short duration of our $\delta^{238}U_{carb}$ record and uncertainties surrounding its interpretation in terms of global and local signals, we think it premature to propose too precise of an environmental history. Nonetheless, it is encouraging that the C-P-U model can simultaneously generate several of

the global changes observed in the latest Devonian, consistent with the hypothesis that the spread of land plants caused at least one transient oceanic anoxic event at this time.

5.4. Marine redox changes and the Hangenberg extinction

Current data support a prolonged duration for the Hangenberg biotic crisis, lasting from the onset of deposition of the Hangenberg black shale in the latest Devonian into the earliest Carboniferous (Kaiser et al., 2008; 2011). The main phase of the Hangenberg Crisis occurred at the base of the Middle *praesulcata* Zone, a level marked by declines in conodonts, ammonoids, trilobites, stromatoporoid sponges, corals, brachiopods, bivalves, and various marine phytoplankton (e.g., Caplan and Bustin, 1999; Kaiser et al., 2016). Climatic cooling and global sea-level changes have been cited as causes of the Hangenberg crisis (e.g., Kaiser et al., 2016), although the pattern of sea-level change during this critical interval is under debate (Johnson et al., 1985; Qie et al., 2015; Kaiser et al., 2016). Furthermore, sedimentological evidence shows that there were sea-level fluctuations before and after deposition of the Hangenberg black shales (Walliser, 1984; Johnson et al., 1985), so a direct role for sea-level changes in the biotic crisis is doubtful. Here, our new $\delta^{238}U$ data highlight that, apart from any changes in sea-surface temperatures and sea-level elevations, the expansion of marine anoxia in latest Devonian oceans is likely to have been a key factor triggering stresses among marine organisms and communities. The expansion of marine anoxia in the upper Lower *Siphonodella praesulcata* Zone coincided with the onset of the Hangenberg biocrisis. This expansion of anoxia was vast enough to have plausibly bathed the outer continental shelves and upper slope areas (i.e., when compared to a situation in the modern oceans where the shelf occupies ~7% of the total ocean floor).

6. Conclusions

We studied $\delta^{238}U$ variations in limestones from the latest Devonian to the earliest Carboniferous in the Long'an section of South China, which preserves a record of the global Hangenberg Crisis. This is the first $\delta^{238}U$ record for the Hangenberg Crisis. The $\delta^{238}U$ profile of the study section shows large secular variations with three negative excursions separated by two positive excursions. We suggest that these positive events are best explained by intensified anoxic/sulfidic conditions in pore fluids during U uptake, which captured ^{238}U-enriched U(IV) in the Long'an carbonates. U isotope mass balance calculations suggest that global marine anoxia expanded strongly in latest Devonian oceans, covering >5% of total global seafloor area and potentially the majority of contemporaneous continental shelves. The expansion of marine anoxia in the upper Lower *praesulcata* Zone coincided with the onset of the Hangenberg Crisis, consistent with a central role for marine anoxia in triggering the extinction event. Global modeling of the coupled C, P, U cycles shows that the spread of seed plants and an associated increased continental to marine P flux could have triggered expansion of marine anoxia in latest Devonian oceans and other global changes, including the positive $\delta^{13}C_{carb}$ excursion and global cooling at that time, but the expansion of anoxia is predicted to have been transient as P solubilization rates and overall weathering intensities declined through internal feedbacks.

Declaration of competing interest

The authors declare that they have no known competing financial interests or personal relationships that could have appeared to influence the work reported in this paper.

Acknowledgements

F.Z. acknowledges support from the National Science Foundation of China (Grant 91955201) and the Danish Council for Independent Research (No. DFF 7014-00295). G.L. was financially supported by the Strategic Priority Research Program of Chinese Academy of Sciences (grant XDB26000000) and National Key R & D Project of China (grant 2016YFA0601104).T.W.D. acknowledges support from the Carlsberg Foundation (grant number CF16-0876). S.Z.S.'s work is supported by the Strategic Priority Research Program (B) (XDB26000000, XDB18000000). T.M.L. was supported by NERC (NE/P013651 and NE/N018508/1). NJP acknowledges funding from the Packard Foundation. Y.C. is supported by internal grant from Montclair State University and the National Science Foundation of China (Grant 41888101). F.Z. and A.D.A. acknowledge funding from the NASA Astrobiology Program (award NNX13AJ71G) and the NSF Frontiers in Earth System Dynamics program (award EAR-1338810).

Appendix A. Supplementary material

Supplementary material related to this article can be found online at https://doi.org/10.1016/j.epsl.2019.115976.

References

Algeo, T.J., Ingall, E., 2007. Sedimentary C_{org}:P ratios, paleocean ventilation, and Phanerozoic atmospheric pO_2. Palaeogeogr. Palaeoclimatol. Palaeoecol. 256 (3), 130–155.

Algeo, T.J., Scheckler, S.E., 1998. Terrestrial-marine teleconnections in the Devonian: links between the evolution of land plants, weathering processes, and marine anoxic events. Philos. Trans. R. Soc. Lond. B, Biol. Sci. 353, 113–130.

Algeo, T.J., Scheckler, S.E., 2010. Land plant evolution and weathering rates changes in the Devonian. Earth Sci., J. China Univ. Geosci. 21 (Suppl. 1), 75–78.

Algeo, T.J., Berner, R.A., Maynard, J.B., Scheckler, S.E., 1995. Late Devonian oceanic anoxic events and biotic crises: "rooted" in the evolution of vascular land plants. GSA Today 5 (3), 63–66.

Andersen, M.B., Romaniello, S., Vance, D., Little, S.H., Herdman, R., Lyons, T.W., 2014. A modern framework for the interpretation of $^{238}U/^{235}U$ in studies of ancient ocean redox. Earth Planet. Sci. Lett. 400, 184–194.

Andersen, M.B., Stirling, C.H., Weyer, S., 2017. Uranium isotope fractionation. Rev. Mineral. Geochem. 82, 799–850.

Banner, J.L., Hanson, G.N., 1990. Calculation of simultaneous isotopic and trace element variations during water-rock interaction with applications to carbonate diagenesis. Geochim. Cosmochim. Acta 54 (11), 3123–3137.

Becker, R., Gradstein, F., Hammer, O., 2012. The Devonian period. In: Gradstein, F.M., Ogg, J.G., Schmitz, M., Ogg, G. (Eds.), The Geologic Time Scale 2012. Elsevier, Amsterdam, pp. 559–601.

Becker, R.T., Königshof, P., Brett, C.E., 2016. Devonian climate, sea level and evolutionary events: an introduction. In: Becker, R.T., Königshof, P., Brett, C.E. (Eds.), Devonian Climate, Sea Level and Evolutionary Events. In: Special Publications, vol. 423. Geological Society, London, pp. 1–11.

Berner, R.A., 1997. The rise of plants and their effect on weathering and atmospheric CO_2. Science 276 (5312), 544–546.

Berner, R.A., Caldeira, K., 1997. The need for mass balance and feedback in the geochemical carbon cycle. Geology 25 (10), 955–956.

Berner, R.A., 2006. GEOCARBSULF: a combined model for Phanerozoic atmospheric O_2 and CO_2. Geochim. Cosmochim. Acta 70 (23), 5653–5664.

Brand, U., Legrand-Blain, M., Streel, M., 2004. Biochemostratigraphy of the Devonian–Carboniferous boundary global stratotype section and point, Griotte formation, La Serre, Montagne Noire, France. Palaeogeogr. Palaeoclimatol. Palaeoecol. 205 (3–4), 337–357.

Caplan, M.L., Bustin, R.M., 1999. Devonian–Carboniferous Hangenberg mass extinction event, widespread organic-rich mudrock and anoxia: causes and consequences. Palaeogeogr. Palaeoclimatol. Palaeoecol. 148 (4), 187–207.

Caves, J.K., Jost, A.B., Lau, K.V., Maher, K., 2016. Cenozoic carbon cycle imbalances and a variable weathering feedback. Earth Planet. Sci. Lett. 450, 152–163.

Chen, X., Romaniello, S.J., Herrmann, A.D., Wasylenki, L.E., Anbar, A.D., 2016. Uranium isotope fractionation during coprecipitation with aragonite and calcite. Geochim. Cosmochim. Acta 188, 189–207.

Chen, X., Romaniello, S.J., Herrmann, A.D., Hardisty, D., Gill, B.C., Anbar, A.D., 2018. Diagenetic effects on uranium isotope fractionation in carbonate sediments from the Bahamas. Geochim. Cosmochim. Acta 237, 294–311.

Clarkson, M.O., Stirling, C.H., Jenkyns, H.C., Dickson, A.J., Porcelli, D., Moy, C.M., Pogge von Strandmann, P.A.E., Cooke, I.R., Lenton, T.M., 2018. Uranium isotope evidence for two episodes of deoxygenation during Oceanic Anoxic Event 2. Proc. Natl. Acad. Sci. USA 115 (12), 2918–2923.

Cole, D.B., Zhang, S., Planavsky, N.J., 2017. A new estimate of detrital redox-sensitive metal concentrations and variability in fluxes to marine sediments. Geochim. Cosmochim. Acta 215, 337–353.

Dahl, T.W., Boyle, R.A., Canfield, D.E., Connelly, J.N., Gill, B.C., Lenton, T.M., Bizzarro, M., 2014. Uranium isotopes distinguish two geochemically distinct stages during the later Cambrian SPICE event. Earth Planet. Sci. Lett. 401, 313–326.

Dahl, T.W., Connelly, J.N., Li, D., Kouchinsky, A., Gill, B.C., Porter, S., Maloof, A.C., Bizzarro, M., 2019. Atmosphere-ocean oxygen and productivity dynamics during early animal radiations. Proc. Natl. Acad. Sci. USA 116 (39), 19352–19361.

Dunk, R.M., Mills, R.A., Jenkins, W.J., 2002. A reevaluation of the oceanic uranium budget for the Holocene. Chem. Geol. 190 (1–4), 45–67.

Henderson, G., Slowey, N., Haddad, G., 1999. Fluid flow through carbonate platforms: constraints from $^{234}U/^{238}U$ and Cl^{-} in Bahamas pore-waters. Earth Planet. Sci. Lett. 169, 99–111.

Ingall, E., Jahnke, R., 1994. Evidence for enhanced phosphorus regeneration from marine sediments overlain by oxygen depleted waters. Geochim. Cosmochim. Acta 58 (11), 2571–2575.

Jacobsen, S.B., Kaufman, A.J., 1999. The Sr, C and O isotopic evolution of Neoproterozoic seawater. Chem. Geol. 161 (1–3), 37–57.

Joachimski, M.M., Buggisch, W., 2002. Conodont apatite $\delta^{18}O$ signatures indicate climatic cooling as a trigger of the Late Devonian mass extinction. Geology 30 (8), 711–714.

Joachimski, M.M., Breisig, S., Buggisch, W., Talent, J.A., Mawson, R., Gereke, M., Morrow, J.R., Day, J., Weddige, K., 2009. Devonian climate and reef evolution: insights from oxygen isotopes in apatite. Earth Planet. Sci. Lett. 284, 599–609.

Johnson, J., Klapper, G., Sandberg, C.A., 1985. Devonian eustatic fluctuations in Euramerica. Geol. Soc. Am. Bull. 96 (5), 567–587.

Kaiser, S.I., Steuber, T., Becker, R.T., Joachimski, M.M., 2006. Geochemical evidence for major environmental change at the Devonian–Carboniferous boundary in the Carnic Alps and the Rhenish Massif. Palaeogeogr. Palaeoclimatol. Palaeoecol. 240 (1–2), 146–160.

Kaiser, S.I., Steuber, T., Becker, R.T., 2008. Environmental change during the Late Famennian and Early Tournaisian (Late Devonian–Early Carboniferous): implications from stable isotopes and conodont biofacies in southern Europe. Geol. J. 43 (2–3), 241–260.

Kaiser, S.I., Becker, R.T., Steuber, T., Aboussalam, S.Z., 2011. Climate-controlled mass extinctions, facies, and sea-level changes around the Devonian–Carboniferous boundary in the eastern Anti-Atlas (SE Morocco). Palaeogeogr. Palaeoclimatol. Palaeoecol. 310 (3–4), 340–364.

Kaiser, S.I., Aretz, M., Becker, R.T., 2016. The global Hangenberg Crisis (Devonian–Carboniferous transition): review of a first-order mass extinction. In: Special Publications, vol. 423. Geological Society, London, pp. 387–437.

Lau, K.V., Maher, K., Altiner, D., Kelley, B.M., Kump, L.R., Lehrmann, D.J., Silva-Tamayo, J.C., Weaver, K.L., Yu, M., Payne, J.L., 2016. Marine anoxia and delayed Earth system recovery after the end-Permian extinction. Proc. Natl. Acad. Sci. USA 113 (9), 2360–2365.

Lau, K.V., Macdonald, F.A., Maher, K., Payne, J.L., 2017. Uranium isotope evidence for temporary ocean oxygenation in the aftermath of the Sturtian Snowball Earth. Earth Planet. Sci. Lett. 458, 282–292.

Lenton, T.M., 2001. The role of land plants, phosphorus weathering and fire in the rise and regulation of atmospheric oxygen. Glob. Change Biol. 7, 613–629.

Liu, J., Qie, W., Algeo, T.J., Yao, L., Huang, J., Luo, G., 2016. Changes in marine nitrogen fixation and denitrification rates during the end-Devonian mass extinction. Palaeogeogr. Palaeoclimatol. Palaeoecol. 448, 195–206.

Liu, J., Luo, G., Lu, Z., Lu, W., Qie, W., Zhang, F., Wang, X., Xie, S., 2019. Shoaling of oxygen minimum zone induced the end Devonian mass extinction. Geochem. Geophys. https://doi.org/10.1029/2019GC008614. In press.

Marynowski, L., Filipiak, P., 2007. Water column euxinia and wildfire evidence during deposition of the Upper Famennian Hangenberg event horizon from the Holy Cross Mountains (central Poland). Geol. Mag. 144 (3), 569–595.

Marynowski, L., Zatoń, M., Rakociński, M., Filipiak, P., Kurkiewicz, S., Pearce, T.J., 2012. Deciphering the upper Famennian Hangenberg Black Shale depositional environments based on multi-proxy record. Palaeogeogr. Palaeoclimatol. Palaeoecol. 346, 66–86.

McArthur, J.M., Howarth, R.J., Shields, G.A., 2012. Strontium isotope stratigraphy. In: Gradstein, F.M., Ogg, J.G., Schmitz, M.D., Ogg, G.M. (Eds.), The Geologic Time Scale 2012. Elsevier, Amsterdam, pp. 127–144.

Qie, W., Liu, J., Chen, J., Wang, X., Mii, H.-s., Zhang, X., Huang, X., Yao, L., Algeo, T.J., Luo, G., 2015. Local overprints on the global carbonate $\delta^{13}C$ signal in Devonian–Carboniferous boundary successions of South China. Palaeogeogr. Palaeoclimatol. Palaeoecol. 418, 290–303.

Romaniello, S.J., Herrmann, A.D., Anbar, A.D., 2013. Uranium concentrations and $^{238}U/^{235}U$ isotope ratios in modern carbonates from the Bahamas: assessing a novel paleoredox proxy. Chem. Geol. 362, 305–316.

Rudnick, R., Gao, S., 2014. Composition of the continental crust. In: Holland, H.D., Turekian, K.K. (Eds.), Treatise on Geochemistry, second ed. Elsevier, Oxford, pp. 1–51.

Sallan, L.C., Coates, M.I., 2010. End-Devonian extinction and a bottleneck in the early evolution of modern jawed vertebrates. Proc. Natl. Acad. Sci. USA 107 (22), 10131–10135.

Scotese, C.R., McKerrow, W.S., 1990. Revised world maps and introduction. In: McKerrow, W.S., Scotese, C.R. (Eds.), Palaeozoic Palaeogeography and Biogeography. In: Geological Society of London Memoir, vol. 12, pp. 1–21.

Tissot, F.L.H., Chen, C., Go, B.M., Naziemiec, M., Healy, G., Bekker, A., Swart, P.K., Dauphas, N., 2018. Controls of eustasy and diagenesis on the $^{238}U/^{235}U$ of carbonates and evolution of the seawater $^{234}U/^{238}U$ during the last 1.4 Myr. Geochim. Cosmochim. Acta 242, 233–265.

Tribovillard, N., Averbuch, O., Devleeschouwer, X., Racki, G., Riboulleau, A., 2004. Deep water anoxia over the Frasnian–Famennian boundary (La Serre, France): a tectonically induced oceanic anoxic event? Terra Nova 16, 288–295.

Tribovillard, N., Algeo, T.J., Lyons, T., Riboulleau, A., 2006. Trace metals as paleoredox and paleoproductivity proxies: an update. Chem. Geol. 232, 12–32.

Veizer, J., Ala, D., Azmy, K., Bruckschen, P., Buhl, D., Bruhn, F., Carden, G.A.F., Diener, A., Ebneth, S., Godderis, Y., Jasper, T., Korte, C., Pawellek, F., Podlaha, O., Strauss, H., 1999. $^{87}Sr/^{86}Sr$, $\delta^{13}C$ and $\delta^{18}O$ evolution of Phanerozoic seawater. Chem. Geol. 161, 59–88.

Walliser, O.H., 1984. Pleading for a natural D/C boundary. Cour. Forschungsinst. Senckenberg 67, 241–246.

White, D.A., Elrick, M., Romaniello, S., Zhang, F., 2018. Global seawater redox trends during the Late Devonian mass extinction detected using U isotopes of marine limestones. Earth Planet. Sci. Lett. 503, 68–77.

Zhang, F., Algeo, T.J., Romaniello, S., Cui, Y., Zhao, L., Chen, Z.Q., Anbar, A.D., 2018a. Congruent Permian-Triassic $\delta^{238}U$ records at Panthalassic and Tethyan sites: confirmation of global oceanic anoxia and validation of the U-isotope paleoredox proxy. Geology 46 (4), 327–330.

Zhang, F., Romaniello, S.J., Algeo, T.J., Lau, K.V., Clapham, M.E., Richoz, S., Herrmann, A.D., Smith, H., Horacek, M., Anbar, A.D., 2018b. Multiple episodes of extensive oceanic anoxia linked to global warming and continental weathering following the latest Permian mass extinction. Sci. Adv. 4 (4), e1602921.

Zhang, F., Xiao, S., Kendall, B., Romaniello, S.J., Cui, H., Meyer, M., Gilleaudeau, G.J., Kaufman, A.J., Anbar, A.D., 2018c. Extensive marine anoxia during the terminal Ediacaran Period. Sci. Adv. 4, eaan8983.

Zhang, F., Algeo, T.J., Cui, Y., Shen, J., Song, H.Y., Sano, H., Rowe, H.D., Anbar, A.D., 2019a. Global-ocean redox variation across the Smithian-Spathian boundary linked to concurrent climatic and biotic changes. Earth-Sci. Rev. 195, 147–168.

Zhang, F., Xiao, S., Romaniello, S.J., Hardisty, D., Li, C., Melezhik, V., Pokrovsky, B., Cheng, M., Shi, W., Lenton, T.M., Anbar, A.D., 2019b. Global marine redox changes drove the rise and fall of the Ediacara biota. Geobiology 17 (6), 594–610.